J-integral Decomposition Approach for 3-D Elasto-Plastic Fatigue Crack Growth Simulations

***M. Kumar, I.V. Singh, and B.K. Mishra**

Department of Mechanical and Industrial Engineering,
Indian Institute of Technology Roorkee, Roorkee 247667 India

*Presenting author: mkumar2@me.iitr.ac.in

Abstract

In the present work, elasto-plastic fatigue crack growth (FCG) in three-dimensional (3D) domains is numerically performed using the extended finite element method (XFEM). The XFEM does not require conformal mesh and remeshing for crack growth modeling as required in the standard finite element method. The crack front in 3D is modeled by joining the small size line segments. The fatigue crack growth rate (FCGR) is computed by the stress intensity factor (SIF) dependent Paris Law. The main challenge in the elasto-plastic FCG modeling is the evaluation of three modes of SIFs, which is properly handled by the *J*-decomposition approach. The field variables are decomposed into their symmetric and anti-symmetric portions across the crack surface in the *J*-decomposition approach. These decomposed portions of fields are used to compute the symmetric and anti-symmetric *J*-integrals. The numerical issues such as the derivative of stress and strain energy density; evaluation of stress in the virtual domain during the *J*-integral calculation are properly addressed. The numerically predicted FCG behavior of Ni-based superalloy is validated experimentally at elevated temperature.

Keywords: Stress intensity factor; Fatigue crack growth (FCG); *J*-decomposition; XFEM.

Introduction

Advancement in the industries and technologies demands the highly efficient and reliable design of the structures/components. To fulfill this objective, all the complex loading effect, environmental factors, flaws in materials like heterogeneity, micro-defects, cracks are necessary to involve in the designing phase. In general, finite element method (FEM) is employed to assist the designing process of the structures/components but FEM is not suitable for designing when material flaws like cracks are considered in the structures/components. In FEM, there is the need of conformal mesh about the crack surface to produce the jump effect in displacement and a very fine mesh is required to capture the stress singularity at the crack front. The modeling to crack propagation requires the remeshing with every crack growth and transfer of data from old mesh to the new mesh. The remeshing procedure is a time-consuming process and data transfer introduces the inaccuracies in the solution. All these complications inspired the researchers to develop new methods to overcome these issues.

In the past two decades, many numerical methodologies are developed by the researchers to overcome the problem of conformal mesh and remeshing for crack modeling such as boundary element method [1], meshfree methods [2]-[3], extended finite element method [4]-[5], extended isogeometric analysis [6]-[7], coupled meshfree and finite element method [8], gradient damage

models [9], phase field method [10] and many more. Among these methods, XFEM is one of the most robust and successfully implemented method to model the stationary cracks, elasto-plastic fatigue crack growth [11], creep crack growth [12], crack growth in heterogeneous materials [13], dynamic crack growth [14], etc. In XFEM, two types of enrichment functions are added to the standard FEM displacement approximation via the partition of unity. The jump enrichment function is utilized to model the jump in displacement field about the crack surface whereas the crack front singularity is captured by the front enrichment functions.

In this paper, the methodology to model the elasto-plastic FCG in the 3D domain is presented. The SIF depended Paris Law is used to calculate the FCGR at the ends of the line segments of the crack front. The individual modes of SIFs are evaluated using the *J*-decomposition approach [15]. All the fields i.e. strain, stress and displacement derivatives are decomposed into symmetric and anti-symmetric portions across the crack surface in this approach. A virtual cylindrical domain is created at the ends of the line segments of crack front to calculate the *J*-integral. The interpolation functions are used to calculate all the required fields at the virtual domain from the nodal data. However, the stress field cannot be obtained by directly interpolation due to plasticity thus; a data transfer scheme is employed to calculate the stress field at the virtual domain. Due to the presence of plasticity, direct derivatives of stress and strain energy density are not possible hence function approximation is utilized to compute the derivative of stress and strain energy density. The numerically computed FCG for Ni-based superalloy is compared with the experimental results and found in a good match.

Mathematical Formulation

In this section, XFEM based methodology to simulate the elasto-plastic FCG is explained. The FCGR is computed by SIF range based Paris Law. The individual modes of SIF are calculated by the *J*-decomposition approach, which depends on the decomposed fields. During the evaluation of *J*-integral, several numerical issues are faced that are discussed in detail in this section. The maximum principal stress criterion is used to obtain the crack growth direction.

Governing Equations

A residual stress-free domain of isotropic homogeneous material is considered for the formulation. The domain is assumed of volume Ω and bounded by the surface Γ as shown in Fig. 1. Prescribed traction and displacement is applied to the surface Γ_t and Γ_u of the domain respectively. A sharp traction free crack in the domain is also considered and denoted by the Γ_c in Fig. 1. The equilibrium equation and the associated boundary conditions for the domain are defined as

$$\sigma_{ij,j} = 0 \quad \text{in} \quad \Omega \quad \forall\ i, j \in \{1,2,3\} \tag{1}$$

$$\sigma_{ij} n_j = 0 \quad \text{on} \quad \Gamma_c \tag{2}$$

$$\sigma_{ij} n_j = \bar{t}_i \quad \text{on} \quad \Gamma_t \tag{3}$$

$$u_i = \bar{u}_i \quad \text{on} \quad \Gamma_u \tag{4}$$

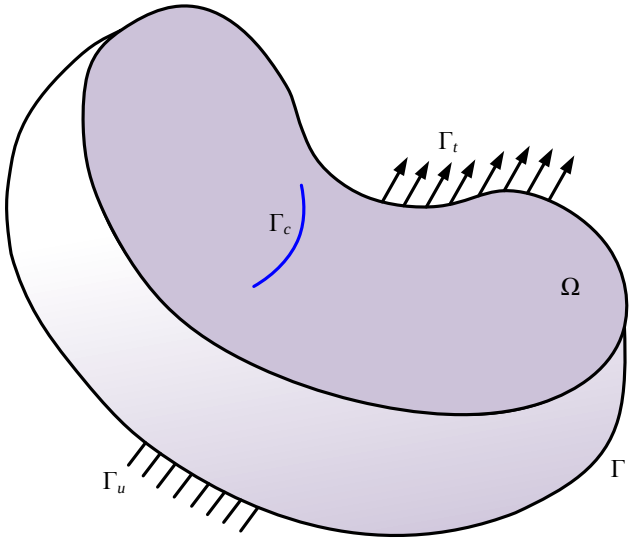

Figure 1. An illustration on 3D cracked domain along with boundary conditions

where σ_{ij} is the Cauchy stress, u_i is the displacement, n_j is the unit normal vector, $\bar{u}_i$ and $\bar{t}_i$ are the applied displacement and traction on the surface Γ_u and Γ_t respectively. The strong form of Eq. (1) is converted into weak form by employing the principle of virtual work as

$$\int_{\Omega} \sigma_{ij} \left(\delta u_i\right)_{,j} d\Omega - \int_{\Gamma_t} \bar{t}_i \delta u_i d\Gamma = 0 \tag{5}$$

This weak form of equilibrium equation is written into discrete equations using discretization of the domain as follows

$$\mathop{\mathrm{A}}_{e=1}^{n_e} \int_{\Omega_e} \mathbf{B}^T \mathbf{C} \mathbf{B} u_i d\Omega - \int_{\Gamma_t} \mathbf{N}^T \bar{t}_i d\Gamma = 0 \tag{6}$$

where $\mathbf{B}$ is the gradient matrix of shape functions, $\mathbf{C}$ is the elasto-plastic constitutive matrix, n_e is the number of elements and $\mathbf{N}$ is the shape function vector. The simultaneous solution of Eq. (6) gives the displacement field that is further used to compute the strain and trial stress field using displacement derivatives and constitutive relation respectively. The trial stress is checked for yielding at each integration point via *J*2 plasticity yielding criterion. For the yielded integration point, generalized Ramberg-Osgood material model along with associated flow rule is used to calculate the plastic strain and stress field [16] whereas for non-yielded integration point trial stress is taken as final stress field. The equilibrium of the system is ensured by the global convergence parameter that is defined as follows

$$\Upsilon = \frac{\left\| \mathbf{F}_{ext} - \mathbf{F}_{int} \right\|}{\left\| \mathbf{F}_{ext} \right\|} \quad \textit{where} \quad \mathbf{F}_{ext} = \int_{\Gamma_t} \mathbf{N}^T \bar{t}_i d\Gamma \; ; \; \mathbf{F}_{int} = \mathop{\mathrm{A}}_{e=1}^{n_e} \int_{\Omega_e} \mathbf{B}^T \sigma_{ij} d\Omega \tag{7}$$

If the convergence parameter is less than the tolerance that means the equilibrium has been attained and the next load step is initiated, otherwise solution of the discrete equations is performed again with the updated residual force and updated elasto-plastic constitutive matrix $(\mathbf{D})$ as

$$\mathop{\mathrm{A}}_{e=1}^{n_e}\int_{\Omega_e}\mathbf{B}^T\mathbf{D}\mathbf{B}u_i d\Omega=\int_{\Gamma_t}\mathbf{N}^T\bar{t}_i d\Gamma-\mathop{\mathrm{A}}_{e=1}^{n_e}\int_{\Omega_e}\mathbf{B}^T\sigma_{ij}d\Omega \tag{8}$$

This process is continued until the convergence is achieved. If the solution diverges then load step is taken as half and the solution of discrete equations is computed from the previously converged load step.

Extended Finite Element Method

XFEM has been successfully used to model the propagating cracks without the need of conformal mesh and remeshing of the domain during crack propagation. In this method, two types of enrichment are added to the standard FEM displacement approximation via the partition of unity. The jump enrichment function is used to model the crack surface whereas the crack front singularity is mimicked by the front enrichment functions. Due to the introduction of these enrichment functions, the total number of degree of freedom (DOF) of the system increased slightly. The enriched displacement approximation for a domain [17] can be written as

$$\mathbf{u}^h(\mathbf{x})=\sum_{i\in n}N_i(\mathbf{x})\mathbf{u}_i+\sum_{j\in n_c}N_j\left[H(\mathbf{x})-H(\mathbf{x}_j)\right]\alpha_j+\sum_{k\in n_t}N_k\sum_{l=1}^{4}\left[\varsigma_l(\mathbf{x})-\varsigma_l(\mathbf{x}_k)\right]\beta_k^l \tag{9}$$

where $H(\mathbf{x})$ and $\varsigma_l(\mathbf{x})$ are the jump and front enrichment functions respectively; n, n_c and n_t presents all the nodes in the domain, nodes associated with completely cut elements and nodes associated with partially cut elements respectively; α and β are the DOFs related with jump enrichment function and front enrichment function respectively. The jump enrichment function and front enrichment function [18] are given below

$$H(\mathbf{x})=\begin{cases}-1 & \text{for } \Psi(\mathbf{x})<0\\ 1 & \text{for } \Psi(\mathbf{x})<0\end{cases} \tag{10}$$

$$\varsigma(\mathbf{x})=\left[r^\eta cos\frac{\theta}{2},r^\eta sin\frac{\theta}{2},r^\eta cos\frac{\theta}{2}sin\theta,r^\eta sin\frac{\theta}{2}sin\theta\right]\qquad\forall\ \eta=\frac{1}{\bar{n}+1} \tag{11}$$

where $\Psi(\mathbf{x})$ is the normal distance from the crack surface; $\bar{n}$ is the hardening constant of material; r and θ are the polar coordinates with respect to crack front. To trace the crack surface in the domain level set is used.

Fatigue Crack Growth

The Paris law is used to estimate the FCGR in the domain as

$$\frac{da}{dN} = C\left(\Delta K_{I\,eq}\right)^{m} \tag{12}$$

where da is the crack growth, dN is the number of cycles required for the crack growth da, $\Delta K_{I\,eq}$ is the equivalent SIF range, C and m are the Paris law constants. The equivalent stress intensity factor range for the constant amplitude fatigue loading is defined as

$$\Delta K_{I\,eq} = K_{I\,eq}^{max} - K_{I\,eq}^{min} \tag{13}$$

where $K_{I\,eq}^{max}$ and $K_{I\,eq}^{min}$ are the equivalent stress intensity factor corresponding to σ^{max} and σ^{min} of applied fatigue load. The individual modes of SIFs (mode-I and mode-II) are used to compute the equivalent stress intensity factor as

$$K_{I\,eq} = K_I\, cos^3\left(\frac{\theta_c}{2}\right) - 3K_{II}\, cos^2\left(\frac{\theta_c}{2}\right) sin\left(\frac{\theta_c}{2}\right) \tag{14}$$

where K_I and K_{II} are the SIFs of mode-I and mode-II respectively that are evaluated by *J*-decomposition approach, θ_c is the critical angle for crack growth. The maximum principal stress criterion [19] is used to compute the critical angle for crack growth as given below

$$\theta_c = 2\,tan^{-1}\left(\frac{1}{4}\frac{K_I}{K_{II}} - \frac{1}{4}\sqrt{\left(\frac{K_I}{K_{II}}\right)^2 + 8}\right) \tag{15}$$

J-decomposition Approach

The individual modes of SIFs are evaluated from *J*-integral, which is calculated at the ends of the crack front line segments using the *J*-decomposition approach [20]. A virtual cylindrical domain as shown in Fig. 2 is created at these ends of crack front to perform the *J*-integral computation. The decomposed form of *J*-integral at these ends is defined as

$$\begin{aligned} J^N = \frac{1}{2L_e}\Bigg(&\int_\Lambda \left(\sigma_{ij}^N \left(u_{i,1}\right)^N - W^N \delta_{1j}\right) q_{,j}\, d\Lambda + \int_\Lambda \left(\sigma_{ij}^N \left(u_{i,1j}\right)^N - W_{,1}^N\right) q\, d\Lambda \\ &+ \int_\Lambda \left(\sigma_{i1,1}^N + \sigma_{i2,2}^N\right)\left(u_{i,1}\right)^N d\Lambda - \int_\Lambda \sigma_{i3}^N \left(u_{i,13}\right)^N d\Lambda\Bigg) \qquad \forall\, N \in \{I, II, III\} \end{aligned} \tag{16}$$

where I, II, III represent the mode-I, mode-II and mode-III respectively, W is the strain energy density, L_e is the length of the virtual domain along the crack front, q is function having value one at the crack front and zeros at the boundary of the virtual domain. The symmetric portion of fields provides the mode-I SIF whereas anti-symmetric portion is further divided to obtain the mode-II and mode-III SIFs.

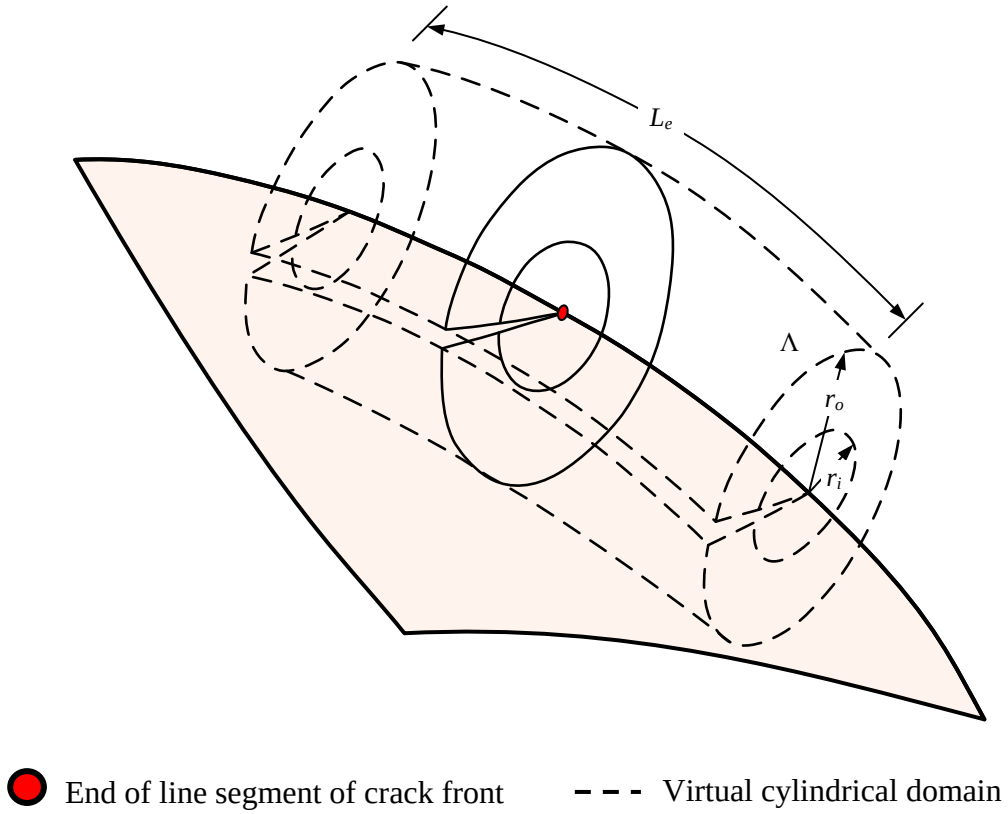

Figure 2. A virtual domain at the end of crack front line segment for the calculation of *J*-integral

In order to compute the *J*-integral by this approach, the required fields are interpolated from the original mesh to the virtual cylindrical domain via shape function interpolation and decomposed into symmetric and anti-symmetric portions across the crack surface. For the decomposition of fields, all the fields are required at the mirror point of the integration point that can be calculated from the nodal data by interpolation functions. Due to the presence of plasticity, stress field cannot be directly obtained at the virtual domain and mirrored point from the displacement field. Therefore, to calculate the stress field at the required point, a data transfer scheme is utilized. In this scheme, the stress field is transferred from the integration points to the nodes [21] by

$$\chi_n = \left(\bar{\mathbf{N}}^T \bar{\mathbf{N}}\right)^{-1} \bar{\mathbf{N}}^T \chi_{ip} \tag{17}$$

where $\bar{\mathbf{N}}^T$ is the matrix contains the value of shape functions at the integration points, χ_n and χ_{ip} are the fields at node and integration point respectively. After that, the nodal stress is interpolated at the required point using shape functions of the element. Due to the use of sub-tetrahedralization for enriched elements, the stress field is extrapolated at the nodes of sub-tetrahedron using Eq. (17) and stored for each tetrahedron separately. The interpolation of the stress field in the enriched element is performed in two steps. In the first step, sub-tetrahedron is identified that contains the mirrored point while in the second step; the stress field is interpolated using the extrapolated nodal

stress and shape functions of the identified sub-tetrahedron. The decomposed stress field for all the modes at the spatial point *P* across the crack surface 1-3 (as given in Fig. 3) is expressed as

$$\sigma_{ij\,P}^{I} = \begin{Bmatrix} \sigma_{11\,P}^{S} \\ \sigma_{22\,P}^{S} \\ \sigma_{33\,P}^{S} \\ \sigma_{12\,P}^{S} \\ \sigma_{23\,P}^{S} \\ \sigma_{13\,P}^{S} \end{Bmatrix} = \frac{1}{2} \begin{Bmatrix} \sigma_{11\,P} + \sigma_{11\,P'} \\ \sigma_{22\,P} + \sigma_{22\,P'} \\ \sigma_{33\,P} + \sigma_{33\,P'} \\ \sigma_{12\,P} - \sigma_{12\,P'} \\ \sigma_{23\,P} - \sigma_{23\,P'} \\ \sigma_{13\,P} + \sigma_{13\,P'} \end{Bmatrix} \tag{18}$$

$$\sigma_{ij\,P}^{II} + \sigma_{ij\,P}^{III} = \begin{Bmatrix} \sigma_{11\,P}^{AS} \\ \sigma_{22\,P}^{AS} \\ \sigma_{33\,P}^{AS} \\ \sigma_{12\,P}^{AS} \\ 0 \\ 0 \end{Bmatrix} + \begin{Bmatrix} 0 \\ 0 \\ 0 \\ 0 \\ \sigma_{23\,P}^{AS} \\ \sigma_{13\,P}^{AS} \end{Bmatrix} = \frac{1}{2} \begin{Bmatrix} \sigma_{11\,P} - \sigma_{11\,P'} \\ \sigma_{22\,P} - \sigma_{22\,P'} \\ \sigma_{33\,P} - \sigma_{33\,P'} \\ \sigma_{12\,P} + \sigma_{12\,P'} \\ 0 \\ 0 \end{Bmatrix} + \frac{1}{2} \begin{Bmatrix} 0 \\ 0 \\ 0 \\ 0 \\ \sigma_{23\,P} + \sigma_{23\,P'} \\ \sigma_{13\,P} - \sigma_{13\,P'} \end{Bmatrix} \tag{19}$$

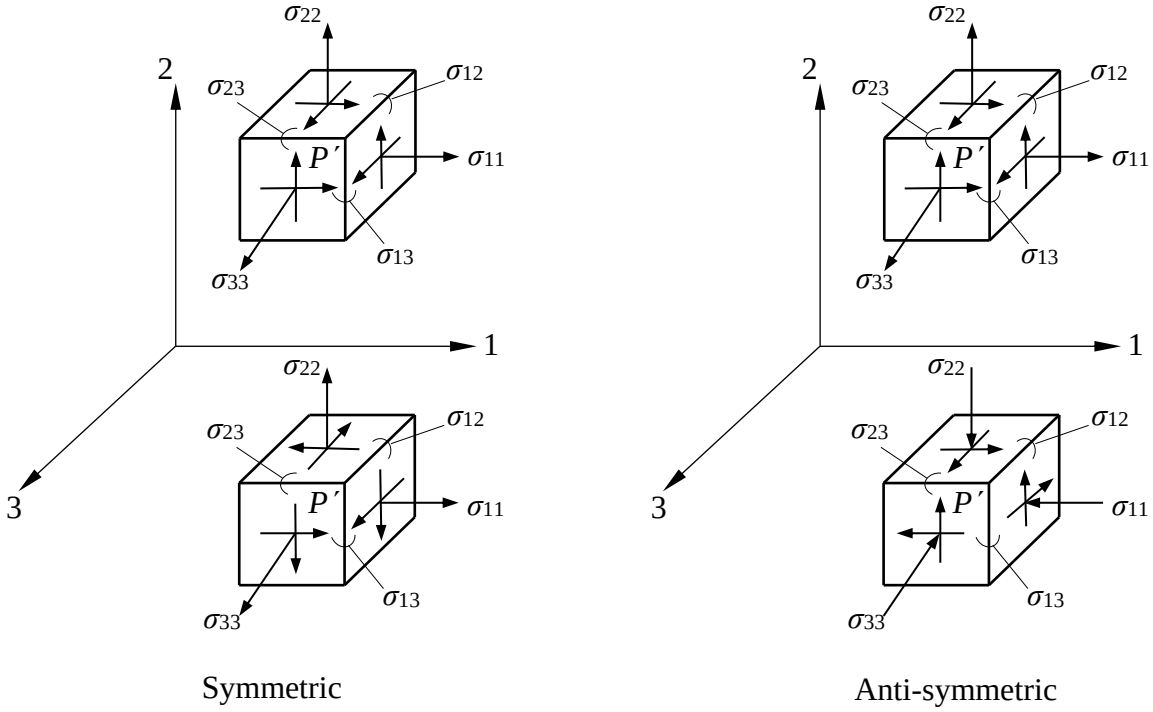

Figure 3. Symmetric and anti-symmetric portion of stress field across the crack surface (1-3) at point *P*

In a similar way, other fields can also be decomposed [22]. The analytical derivatives of strain energy density and stress are not possible due to the plasticity hence; it is evaluated by the function approximation. The required field of all the integration points of an element is fitted into a quadratic function by nonlinear least squares method as

$$\varpi^N = f_1 + f_2\xi + f_3\eta + f_4\zeta + f_5\xi^2 + f_6\eta^2 + f_7\zeta^2 + f_8\xi\eta + f_9\eta\zeta + f_{10}\xi\zeta \tag{20}$$

where ξ,η,ζ are the local coordinates of the integration points and $f_1, f_2, f_3, f_4, f_5, f_6, f_7, f_8, f_9, f_{10}$ are the fitting constants. The derivative of Eq. (20) is used to compute the derivative of stress and strain energy density.

Numerical Implementation

The flowchart for the implementation of the FCG methodology is presented in Fig. 4. The discretized domain along with boundary conditions is given as input to the computational model. The crack front is divided into small line segments to perform the simulation. The elasto-plastic solution is performed on the computational model using a typical load step as discussed in the previous section. After obtaining the converged solution on complete loading, a virtual cylindrical domain is created at the ends of the line segments of crack front to evaluate the *J*-integral using the *J*-decomposition approach. The data is transferred from the original mesh to the virtual cylindrical domain to compute the *J*-integral. The stress evaluation at the virtual domain and mirror point is performed via the data transfer scheme. The derivatives of stress and strain energy density are computed by function approximation as given in Eq. (20). The decomposed fields are used to calculate the *J*-integral for all the modes, which are further converted into SIFs of individual modes as

$$K_i = \sqrt{\bar{E}\, J^i} \qquad \forall \; i \in \{I, II\} \tag{21}$$

$$K_{III} = \sqrt{2\bar{G}\, J^{III}} \tag{22}$$

where $\bar{E}$ and $\bar{G}$ is the Young's modulus (for plane stress condition) and shear modulus respectively. The equivalent SIF and critical angle are calculated from the SIFs of individual modes. The crack growth rate at the ends of line segments of the crack front is evaluated using equivalent SIF range and the Paris Law. The crack increment is computed for a particular number of cycles and the current crack front is updated with this crack increment. For the next step of the analysis, the updated crack front is considered as the crack front and the whole process of loading and calculation of SIF is repeated. This process is continued until the equivalent SIF is less than the fracture toughness.

Numerical Results and Discussion

A compact tensile specimen consists of Ni-based superalloy having 32 mm width and 6 mm thickness is considered for the validation of the presented FCG methodology. A through crack of 7.2 mm is considered in the specimen as shown in Fig. 5.

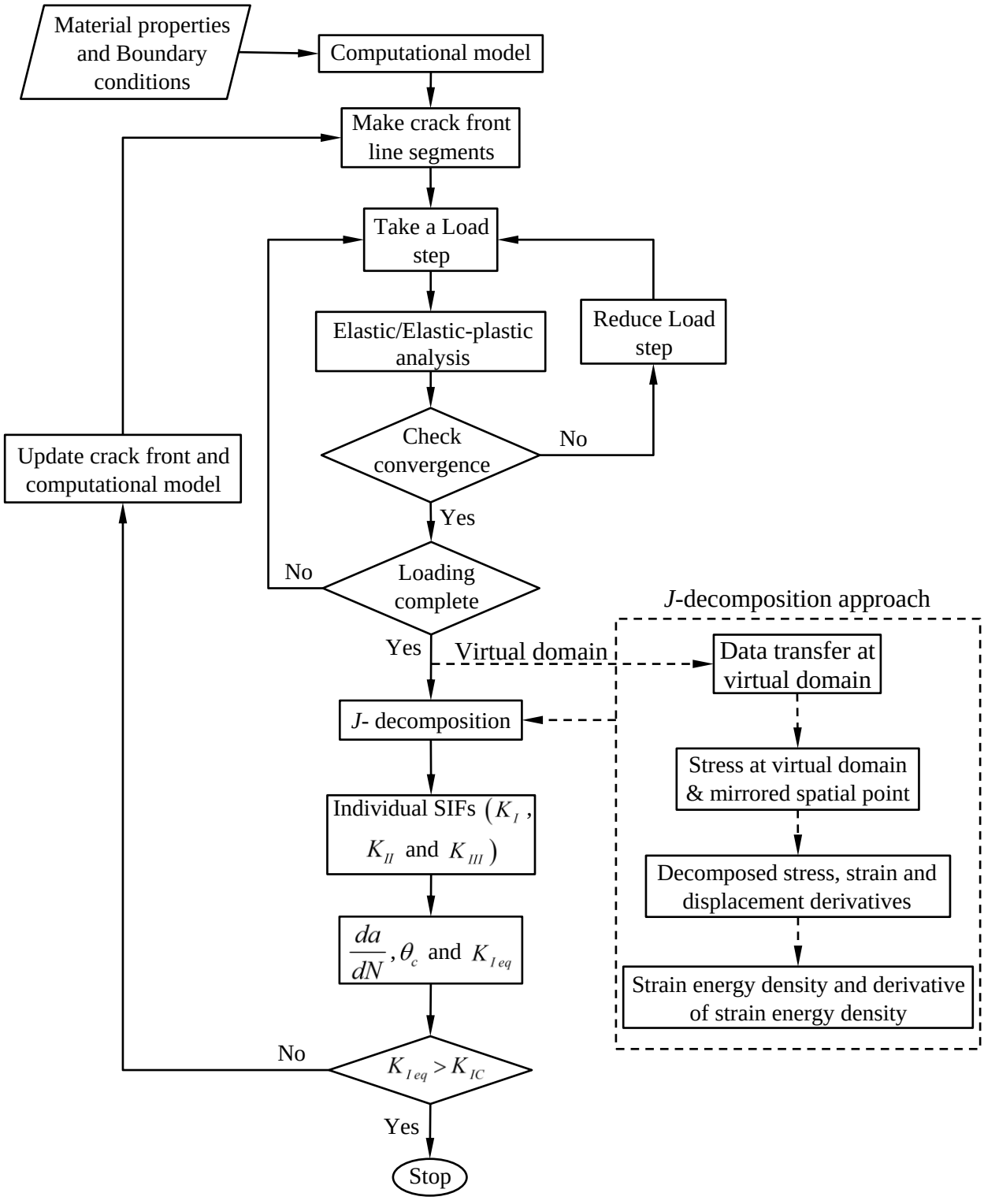

Figure 4: The flowchart for the implementation of proposed FCG methodology

The fatigue load of $F_{max} = 3500\,\text{N}\ (R = 0.1)$ is applied at the elevated temperature of 650 °C. The mechanical and fatigue properties of Ni-based superalloy at the elevated temperature are provided in Table 1. The specimen is discretized into 15 × 15 × 3 elements while the crack front is divided into 8 line segments. A virtual cylindrical domain is created at the endpoints of the line segments of crack front except for the corner points of the crack front. The radius and length of the virtual cylindrical domain are taken as 1 mm and 0.5 mm respectively. The decomposed fields are used to calculate the individual modes of SIFs as described in the previous sections.

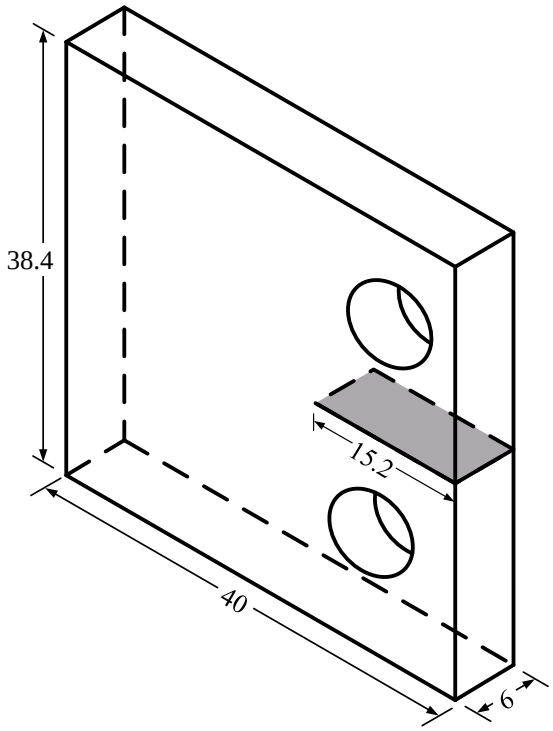

Figure 5. A schematic of compact tensile specimen considered for simulation

Table 1. Material properties of Ni-based superalloy at 650 °C

Mechanical Properties	**650 ºC Value**
Young's modulus, E (GPa)	180
Poisson ratio, v	0.33
Yield strength, σ_{yts} (MPa)	653
Ultimate tensile strength, σ_{uts} (MPa)	987
Paris Law constant, C	1.78×10^{-8}
Paris Law constant, m	2.89

The crack growth is evaluated from the crack growth rate at each endpoint of line segments of crack front for a particular number of cycles. Initially, the number of cycles is kept high but when the crack growth is in the range of element size then the number of cycles is reduced to capture the very high rate of crack growth. The numerically computed FCG is shown in Fig. 6 and compared with the experimental results [23]. The numerical results are found in a good agreement with the experimental results. The numerically obtained crack front at different stages of the simulation is also presented in Fig. 7. The predicted growth of the crack front in the middle of the specimen is high as compared to the surface of the specimen, which is consistent with the theoretical expectations.

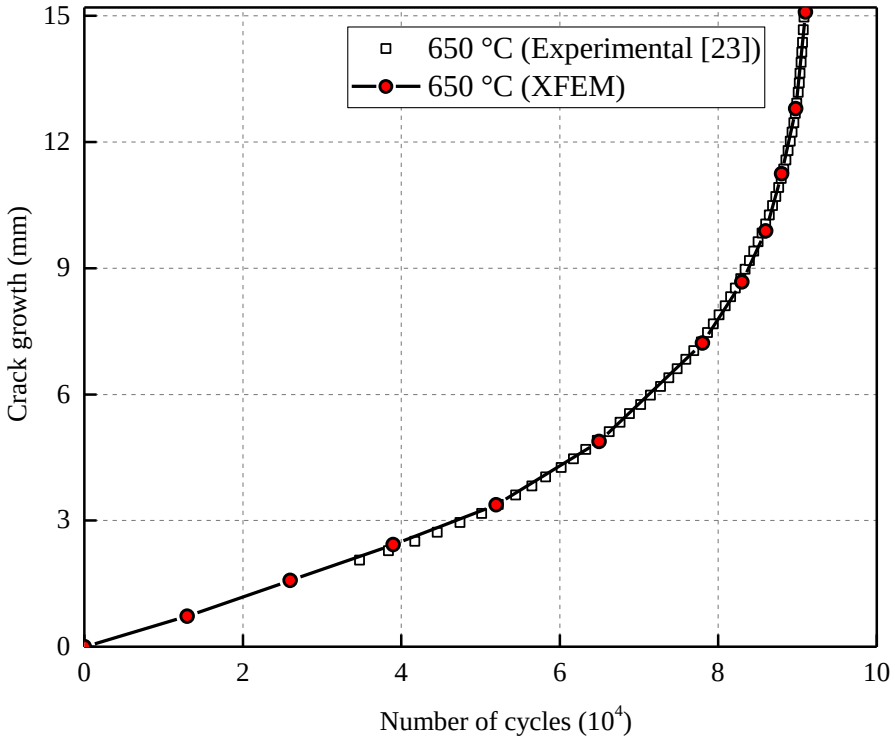

Figure 6. A comparison of numerically predicted fatigue crack growth and experimental results for Ni-based superalloy at elevated temperature

Summary

In this paper, elasto-plastic FCG in the 3D domain is simulated using the XFEM. In the current study, FCGR is computed by the SIF based Paris law. The SIFs of individual modes at the ends of the line segments of the crack front are calculated via *J*-integral through *J*-decomposition approach. The variable fields are decomposed into symmetric and anti-symmetric portions across the crack surface in this approach. A virtual cylindrical domain has created at the ends of the line segments of the crack front to compute the *J*-integral. The nodal data is used to calculate all the required fields at the virtual domain by interpolation functions. In the presence of plastic deformation, the stress field at the virtual domain is obtained by a data transfer scheme. The direct

derivatives of stress and strain energy density are not possible hence function approximation is employed to compute the derivative of stress and strain energy density. The obtained fatigue crack growth for the compact tensile specimen is compared with the experimental results and found in a good match.

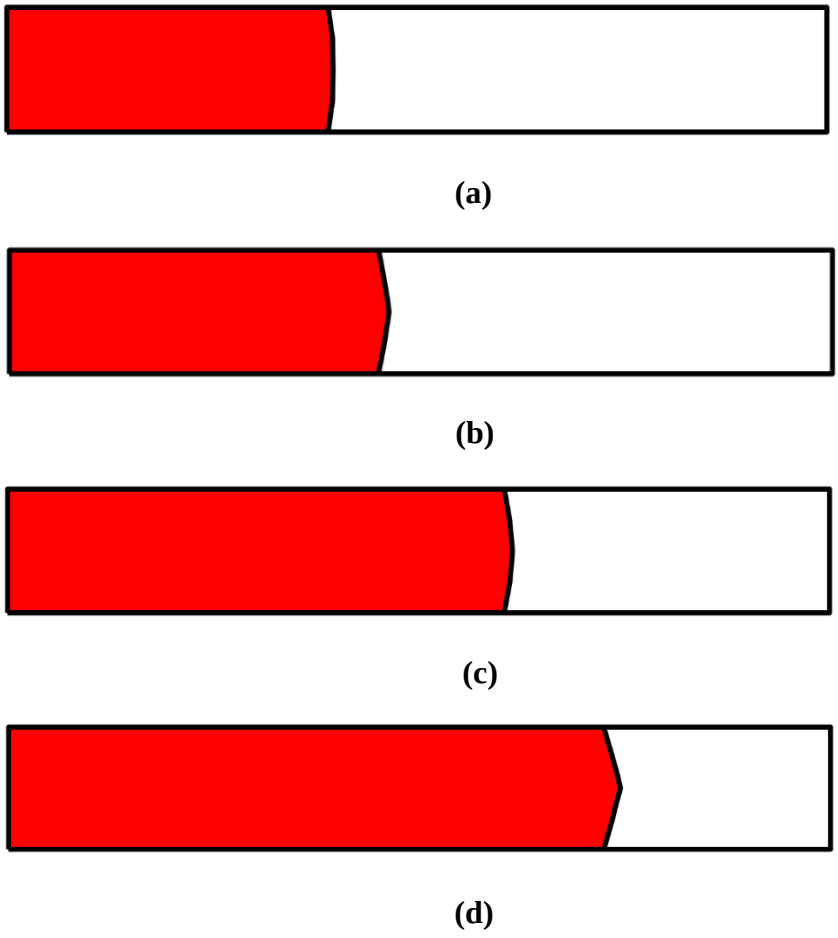

Figure 7. Numerically predicted crack path at different stages of the simulation after (a) 13000 cycles (b) 52000 cycles (c) 86000 cycles (d) 91000 cycles

Acknowledgment

This research work is performed as the part of doctoral work of Mr. Manish Kumar under the fellowship of Ministry of Human Resource and Development, Government of India. This research work is also partially funded by the Alumni Association of Indian Institute of Technology Roorkee, India.

References

[1] Yan, X.Q. (2006) A boundary element modeling of fatigue crack growth in a plane elastic plate, *Mechanics Research Communications* **33**, 470-481.

[2] Belytschko, T., Lu, Y.Y., and Gu, L. (1994) Element-Free Galerkin Methods, *International Journal for Numerical Methods in Engineering* **37**, 229-256.
[3] Pant, M., Singh, I.V., and Mishra, B.K. (2011) Evaluation of mixed mode stress intensity factors for interface cracks using EFGM, *Applied Mathematical Modelling* **35**, 3443-3459.
[4] Belytschko, T. and Black, T. (1999) Elastic crack growth in finite elements with minimal remeshing, *International Journal for Numerical Methods in Engineering* **45**, 601-620.
[5] Singh, I.V., Mishra, B.K., Bhattacharya, S., and Patil, R.U. (2012) The numerical simulation of fatigue crack growth using extended finite element method, *International Journal of Fatigue* **36**, 109-119.
[6] Luycker, E.D., Benson, D.J., Belytschko, T., Bazilevs, Y., and Hsu, M.C. (2011) X-FEM in isogeometric analysis for linear fracture mechanics, *International Journal for Numerical Methods in Engineering* **87**, 541-565.
[7] Singh, S.K., Singh, I.V., Mishra, B.K., Bhardwaj, G., and Singh, S.K. (2018) Analysis of cracked plate using higher-order shear deformation theory: Asymptotic crack-tip fields and XIGA implementation, *Computer Methods in Applied Mechanics and Engineering* **336**, 594-639.
[8] Shedbale, A.S., Singh, I.V., and Mishra, B.K. (2016) A coupled FE–EFG approach for modelling crack growth in ductile materials, *Fatigue & Fracture of Engineering Materials & Structures* **39**, 1204–1225.
[9] Sarkar, S., Singh, I.V., Mishra, B.K., Shedbale, A.S., and Poh, L.H. (2019) A comparative study and ABAQUS implementation of conventional and localizing gradient enhanced damage models, *Finite Elements in Analysis and Design* **160**, 1-31.
[10] Patil, R.U., Mishra, B.K., and Singh, I.V. (2018) A local moving extended phase field method (LMXPFM) for failure analysis of brittle materials, *Computer Methods in Applied Mechanics and Engineering* **342**, 674-709.
[11] Kumar, S., Shedbale, A.S., Singh, I.V., and Mishra, B.K. (2015) Elasto-plastic fatigue crack growth analysis of plane problems in the presence of flaws using XFEM, *Frontiers of Structural and Civil Engineering* **9**, 420-440.
[12] Pandey, V.B., Singh, I.V., Mishra, B.K., Ahmad, S., Rao, A.V., and Kumar, V. (2019) Creep crack simulations using continuum damage mechanics and extended finite element method, *International Journal of Damage Mechanics* **28**, 3-34.
[13] Patil, R.U., Mishra, B.K., and Singh, I.V. (2017) A new multiscale XFEM for the elastic properties evaluation of heterogeneous materials, *International Journal of Mechanical Sciences* **122**, 277-287.
[14] Kumar, S., Singh, I.V., Mishra, B.K., and Singh, A. (2016) New enrichments in XFEM to model dynamic crack response of 2-D elastic solids, *International Journal of Impact Engineering* **87**, 198-211.
[15] Rigby, R.H. and Aliabadi, M.H. (1998) Decomposition of the mixed-mode J-integral - Revisited, *International Journal of Solids and Structures* **35**, 2073-2099.
[16] Kumar, M., Singh, I.V., Mishra, B.K., Ahmad, S., Rao, A.V., and Kumar, V. (2018) Mixed mode crack growth in elasto-plastic-creeping solids using XFEM, *Engineering Fracture Mechanics* **199**, 489-517.
[17] Moës, N., Dolbow, J., and Belytschko, T. (1999) A finite element method for crack growth without remeshing, *International Journal for Numerical Methods in Engineering* **46**, 131-150.
[18] Shedbale, A.S., Singh, I.V., Mishra, B.K., and Sharma, K. (2017) Ductile failure modeling and simulations using coupled FE-EFG approach, *International Journal of Fracture* **203**, 183-209.
[19] Bhardwaj, G., Singh, I.V., and Mishra, B.K. (2015) Fatigue crack growth in functionally graded material using homogenized XIGA, *Composite Structures* **134**, 269-284.
[20] Kumar, M., Bhuwal, A.S., Singh, I.V., Mishra, B.K., Ahmad, S., Rao, A.V., and Kumar, V. (2017) Nonlinear fatigue crack growth simulations using J-integral decomposition and XFEM, *Plasticity and Impact Mechanics* **173**, 1209-1214.
[21] Durand, R. and Farias, M.M. (2014) A local extrapolation method for finite elements, *Advances in Engineering Software* **67**, 1-9.
[22] Kumar, M., Singh, I.V., and Mishra, B.K. (2019) Fatigue Crack Growth Simulations of Plastically Graded Materials using XFEM and J-Integral Decomposition Approach, *Engineering Fracture Mechanics* **216**.
[23] Kumar, M., Ahmad, S., Singh, I.V., Rao, A.V., Kumar, J., and Kumar, V. (2018) Experimental and numerical studies to estimate fatigue crack growth behavior of Ni-based super alloy, *Theoretical and Applied Fracture Mechanics* **96**, 604-616.